

Manuscript: amt-2021-67

Title: "Improved ozone monitoring by ground-based FTIR spectrometry" by Omaira E. García et al., Atmos. Meas. Tech. Discuss., <https://doi.org/10.5194/amt-2021-67-RC1>, 2021

Response to Referee#3

General comments:

The idea of homogenizing the retrieval strategy is convincing. The strategy found at IZO indeed enhances precision when comparing to Brewer data. However, the 5 different strategies do not exhibit important differences (biases) among them and the choice of the optimum strategy should be clarified. Applying the selected strategy to other NDACC measurements to verify whether this optimum strategy could be useful to the FTIR community would make the paper gain in scientific impact.

Overall, the paper is well written and structured but the abstract and conclusion sections are too vague and do not provide a concise and complete summary. These sections would need rephrasing to better highlight the main ideas/results of this work. In addition, figures would need clarity improvements. The number of figures should be reduced to fit the main scientific results.

Specific comments:

If the goal is to derive homogeneous O₃ retrievals strategy within NDACC, why not trying the optimized strategy tested from the IZO dataset to another mid-latitude or polar NDACC measurements? This strategy is applied to IZO measurements, where, as stated in the text, is located in very dry atmospheric conditions. What happen to this optimized strategy when O₃ is monitored in a much more humid environment? What would be the effect of H₂O line interferences?

The authors agree with the Referee in that testing the proposed O₃ set-ups on different NDACC FTIR stations (under different humidity conditions, latitudes, altitudes...) would indeed strengthen the results observed at Izaña Observatory (IZO). That might also motivate the NDACC FTIR community to revise the standard O₃ retrieval strategy. In fact, discussions have already started with different NDACC stations to carry out a harmonised testing. However, this comprehensive study is not a simple matter, and requires reaching a consensus on several important factors among the participating stations, such as the treatment of water vapour interference (one-step and two-step strategies like in the current paper), ILS characterisation, retrieval code (currently two retrieval softwares are used within the FTIR community), retrieval settings (e.g. spectroscopic database), etc.

Given the importance of water vapour absorption across the infrared spectrum, the treatment of H₂O in O₃ retrievals should be carefully considered in the inversion procedure. For that reason, all the O₃ set-ups analysed in the current work are based on a two-step retrieval strategy, which minimises the H₂O interferences, allowing the conclusions drawn to be valid for many more humidity environments. However, the authors agree with both Referees in that the treatment of H₂O and its potential interferences are an important topic and can be treated in greater depth in the paper, leading to more robust conclusions. Accordingly, new information will be added to the revised manuscript as follows:

On the one hand, Figure 2 of the preprint has been modified by including the changes in the FTIR radiances for the spectral micro-windows used for the O_3 retrievals due to different changes in the H_2O content: 50% (total column of 16.1 mm), 100% (total column of 21.5 mm), and 200% (total column of 32.3 mm) (the actual total column is 10.7 mm). These values could account for typical H_2O content and variations at sites with greater humidity (see Figure 1 below). As observed, the spectral signatures of H_2O variations are much stronger in the broad 1000 spectral region than in the narrow micro-windows (4MWs/5MWs), indicating that the quality of the O_3 products in that region strongly depends on a correct interpretation of the spectroscopic H_2O interferences.

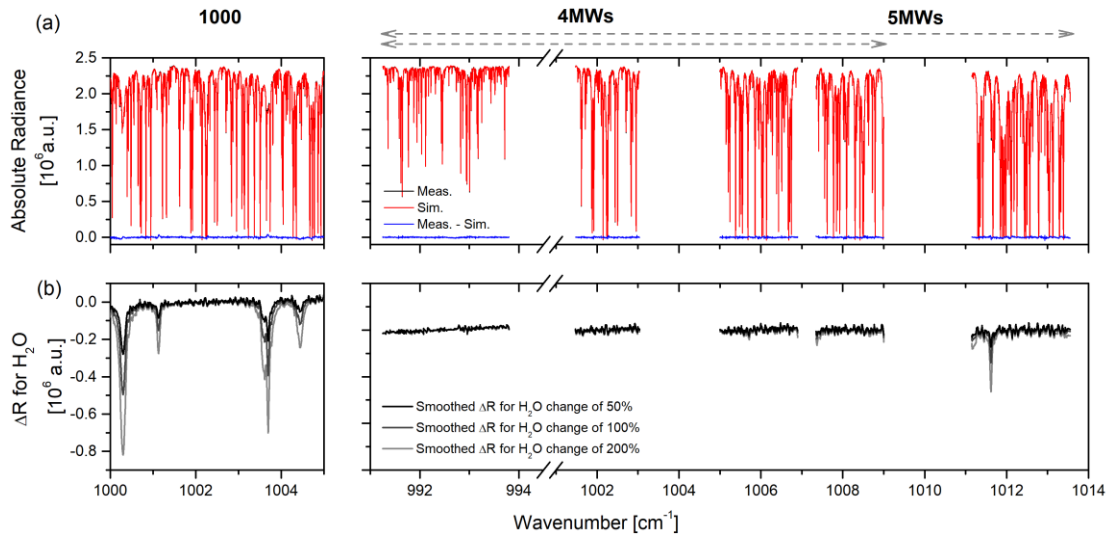


Figure 1: (a) Spectral micro-windows used in the different FTIR O_3 retrieval strategies: broad window used in the set-ups 1000/1000T, encompassing the 1000–1005 cm^{-1} spectral region, and the four and five micro-windows used in the set-ups 4MWs/4MWsT, between ~ 991 and 1009 cm^{-1} , and in 5MWs/5MWsT between ~ 991 and 1014 cm^{-1} , respectively. (b) Spectral changes in the FTIR radiances (ΔR) due to changes in H_2O content of 50% (total column of 16.1 mm), 100% (total column of 21.5 mm), and 200% (total column of 32.3 mm). The actual H_2O total column is 10.7 mm.

On the other hand, the impact of the treatment of H_2O on O_3 retrievals for all O_3 set-ups will be addressed in a dedicated Appendix, using the one-step and two-step retrieval strategies (following Referee#2's comment), where:

1. One-step refers to simultaneously retrieving the H_2O and O_3 profiles, using a Tikhonov-Philips slope constraint for both gases and adding the microwindow of 896.4–896.6 cm^{-1} for a better H_2O determination (as done at the NDACC FTIR Lauder and Wollongong sites in Vigouroux et al., 2015).
2. Two-step refers to the strategy followed in the current paper, where the H_2O a priori profiles are only scaled in the O_3 retrieval but these a priori profiles have been preliminarily retrieved in dedicated H_2O microwindows for each spectrum (Schneider et al., 2012).

The new Appendix will include the theoretical assessment of H_2O cross-interference via H_2O interfering error according to García et al. (2014). As can be seen in Figure 2, the H_2O interfering error is noticeable (less than 0.06%), but not critical. Nevertheless, it has been found that the H_2O interference strongly depends on the spectral region used for the O_3 retrievals (the higher impact is observed for the 1000 spectral region as expected from Figure 1), as well as on the treatment of the atmospheric temperature profile (with or without simultaneous retrieval). Note that the two-

step strategy drastically reduces the H₂O interfering error for those set-ups using narrow micro-windows when the simultaneous temperature fit is included (4MWsT and 5MWsT set-ups), leading to expected errors on the O₃ total columns smaller than 0.01%. The H₂O interfering effect also drops for the 1000 spectral region, but to a lesser extent given the presence of important H₂O absorption lines in that region (see Figure 1 above). These results confirm that using narrow O₃ absorption lines, along with a two-step inversion strategy to estimate the H₂O profile in a dedicated H₂O profile fit prior to the O₃ retrievals result in a superior O₃ strategy.

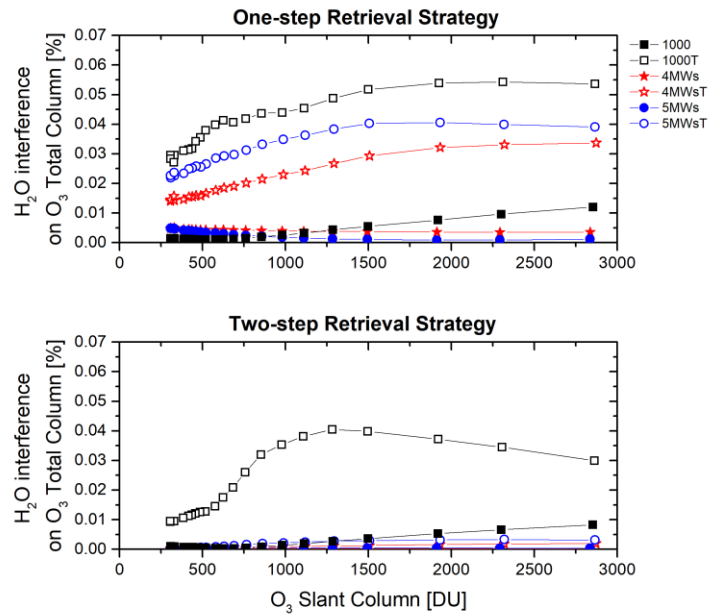


Figure 2. H₂O interfering error on O₃ total columns (in %) for all O₃ set-ups using the one-step and two-step retrieval strategies for the exemplary day used in the paper (31st August 2007).

Additionally, the new Appendix will include the comparison of Brewer observations to FTIR O₃ total columns from the different O₃ set-ups using one-step and two-step retrieval strategies. For the IFS 120M instrument, the spectral region used for O₃ retrievals was measured with two different filters at IZO: SI between 925.30-1379.71 cm⁻¹ and SK between 700.00-1079.71 cm⁻¹. The results presented in the preprint (two-step strategy) were evaluated from measured SI spectra given their higher signal-to-noise ratio. Unfortunately, these spectra do not cover the 896.4–896.6 cm⁻¹ line needed for the H₂O estimation in the one-step strategy, therefore the performance of both strategies has been evaluated here using the measured SK spectra for the 120M period (1999-2004).

As summarised in Table 1, the preliminary H₂O retrievals slightly enhance the quality of the O₃ retrievals with respect to the one-step strategy for all periods and set-ups. The more unstable the instrument, the greater the effect. It is worth highlighting the fact that the differences found between the two strategies are in excellent agreement with the estimated H₂O interfering error values (see Figure 2 above). Note that Table 1 also includes the comparison results for the SI spectra using the two-step retrieval strategy, corroborating the best performance of these spectra for FTIR O₃ retrievals.

	1999-2004	2005-2008	2008-2018	1999-2018
set-up	M[%], σ [%], R			
One-Step Retrieval Strategy (Filter SK for 1999-2004)				
1000	4.13, 2.52, 0.871	4.39, 0.87, 0.971	3.29, 0.83, 0.982	3.38, 1.06, 0.971
4MW _s	4.04, 2.50, 0.873	4.38, 0.86, 0.972	3.29, 0.82, 0.982	3.37, 1.05, 0.971
5MW _s	4.07, 2.44, 0.879	4.40, 0.83, 0.974	3.34, 0.81, 0.983	3.42, 1.02, 0.973
1000T	3.73, 2.21, 0.908	3.92, 0.77, 0.976	3.12, 0.71, 0.987	3.16, 0.89, 0.979
4MW _s T	3.83, 2.16, 0.917	3.94, 0.67, 0.982	3.30, 0.68, 0.988	3.36, 0.84, 0.982
5MW _s T	3.92, 2.08, 0.922	4.07, 0.65, 0.983	3.39, 0.67, 0.988	3.45, 0.83, 0.982
Two-Step Retrieval Strategy (Filter SK for 1999-2004)				
1000	3.98, 2.46, 0.874	4.47, 0.86, 0.970	3.35, 0.83, 0.982	3.45, 1.06, 0.970
4MW _s	3.92, 2.45, 0.875	4.49, 0.85, 0.971	3.34, 0.82, 0.982	3.43, 1.05, 0.971
5MW _s	4.03, 2.38, 0.882	4.53, 0.82, 0.973	3.41, 0.81, 0.983	3.49, 1.02, 0.972
1000T	3.56, 2.21, 0.906	3.79, 0.82, 0.972	3.04, 0.73, 0.986	3.09, 0.90, 0.978
4MW _s T	3.79, 2.14, 0.916	3.97, 0.66, 0.981	3.32, 0.68, 0.988	3.39, 0.84, 0.981
5MW _s T	3.93, 2.06, 0.922	4.15, 0.63, 0.983	3.44, 0.67, 0.988	3.51, 0.83, 0.982
Two-Step Retrieval Strategy (Filter SI for 1999-2004)				
1000	4.29, 1.38, 0.957	4.47, 0.86, 0.970	3.35, 0.83, 0.982	3.46, 0.95, 0.975
4MW _s	4.28, 1.36, 0.959	4.49, 0.85, 0.971	3.34, 0.82, 0.982	3.45, 0.93, 0.976
5MW _s	4.35, 1.32, 0.962	4.53, 0.82, 0.973	3.41, 0.81, 0.983	3.50, 0.91, 0.977
1000T	4.83, 1.97, 0.926	3.79, 0.82, 0.972	3.04, 0.73, 0.986	3.12, 0.90, 0.977
4MW _s T	4.84, 1.90, 0.934	3.97, 0.66, 0.981	3.32, 0.68, 0.988	3.40, 0.83, 0.981
5MW _s T	4.81, 1.82, 0.940	4.15, 0.63, 0.983	3.44, 0.67, 0.988	3.53, 0.81, 0.982

Table 1. Summary of statistics for FTIR-Brewer comparison for the set-ups 1000/1000T, 4MW_s/4MW_sT, and 5MW_s/5MW_sT: median (M, in %) and standard deviation (σ , in %) of the relative differences, and Pearson correlation coefficient (R) of the direct comparison for the periods 1999-2004, 2005-May 2008 and June 2008-2018, and for the entire time series (1999-2018), considering the one-step and two-step strategies for the H₂O estimation.

Therefore, as mentioned above, the authors agreeing on the harmonisation study would be very useful indeed, but we consider it to be such a huge exercise that it should be addressed in two separated works: the first one addressing the comprehensive study performed in the current study (theoretical and experimental quality assessment); and a second work, where the lessons learnt from the first study can be easily applied at different NDACC stations under different casuistry. This reflection will be included in the conclusions of the revised manuscript.

There are too many figures. Some of them could be combined or could go in supplement information content. Figure 4 is very busy and hard to analyze. Figure 6 could be improved: use smaller dots in panel a and other colors in panels b and c since the blue and black lines are difficult to distinguish.

The number and content of the figures will be modified as follows:

- Figure 2 will be replaced by Figure 1 of the current revision.
- Figure 3 will be removed from the revised paper.
- Figure 4 and 5 will be combined in one figure and plots showing the detailed error analysis based on the different error sources will be moved to Appendix A.
- Figure 6 will be improved by following the Referee's suggestions.
- Figure 8 will include scatter plots of Brewer versus FTIR set-ups following Referee#3 comment.

The abstract section needs to be reorganized to focus on the key results. Line 7: "provide consistent results" related to what? Line 15: "it" refers to what?

Sorry for the vaguely-referred information. The authors will make the abstract and conclusions clearer, focusing on the key messages.

In the introduction section, O₃ trend in the stratosphere is well explained. For consistency, it would be useful to explain O₃ trend in the troposphere as well. Line 38: how many NDACC stations are measuring O₃?

Some statements about tropospheric O₃ records will be included in the introduction section as follows (the new text in bold):

"In the troposphere, since O₃ (especially when close to the surface) is highly variable, depending on time period, region, elevation and proximity to fresh O₃ precursor emissions (Gaudel et al., 2018), there is no consistent picture of O₃ tropospheric changes around the world (Steinbrecht2017; Gaudel et al., 2018; WMO, 2018, and references therein). Hence, high-quality and long-term O₃ measurements are essential to further improve our understanding of O₃ response to the natural and anthropogenic forcings, as well as to estimate consistent trends at a global scale (Vigouroux et al., 2015)."

According to the NDACC archive, there have been twenty-two FTIR stations providing O₃ data since the network's creation. Nineteen out of these stations are currently operative and reporting O₃ data to the NDACC database. This information will be included in the revised manuscript.

The seasonal O₃ variability seen by the Brewer and the FTIR observations are different. This could be further analyzed and explain in the text. What about the vertical sensitivities of both dataset?

The temporal and vertical response of the FTIR retrievals on real atmospheric variability can be quantified by the trace of averaging kernels obtained in the retrieval procedure (the so-called degrees of freedom for signal, DOFS). The O₃ DOFS mainly depends on the O₃ absorption signature (O₃ slant column, O₃ SC) and its seasonal behaviour. As seen in Figure 3, the retrieved

total DOFS values are strongly anti-correlated with the O₃ SC amounts. Therefore, the maximum sensitivity of the FTIR system is expected to be found in spring and summer, when the minimum O₃ SC values are reached. The seasonal behaviour observed in the total DOFS comes from the seasonality in the independent O₃ partial columns that can be retrieved by the remote-sensing FTIR system (see Figures 3.b and 3.c). Note that although the FTIR sensitivity depends on the spectral region used for O₃ retrievals (see Table 1 of preprint), similar seasonal patterns are found for all set-ups.

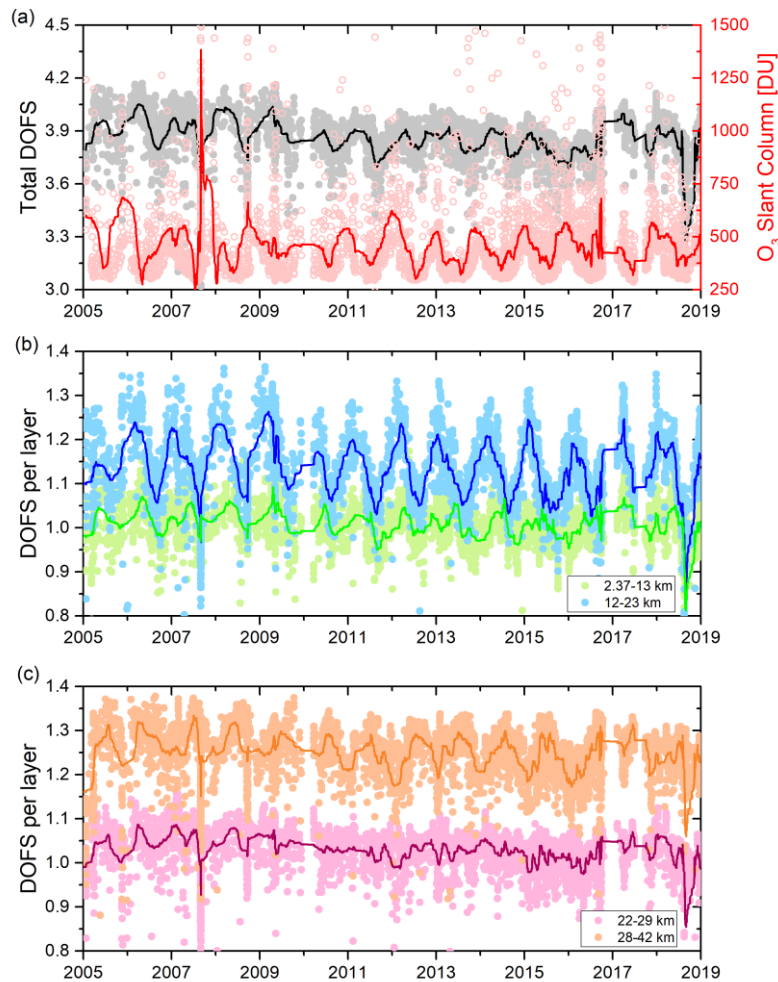


Figure 3. (a) Time series of the total DOFS (black squares) and ozone amount in the slant path [DU] (red circles) for the 1000 set-up between 2005 and 2019 (IFS 120/5 HR). (b) and (c) as for (a), but for the partial columns between 2.37-13 km, 12-23 km, 22-29 km, and 28-42 km. The partial columns are defined according to García et al. (2012).

As regards the Brewer data, Brewer instruments are sensitive to the entire O₃ total column, the seasonal sensitivity being strongly linked to the effective ozone temperature and ozone height assumed in the data processing (Redondas et al., 2014; Gröbner et al., 2021). As stated in the preprint, the Brewer O₃ TCs used in the current work have been computed using the so-called effective O₃ cross-sections throughout the atmosphere (Bass and Paur, 1985), corresponding to a fixed effective O₃ height of 22 km and a fixed effective temperature of the O₃ layer of -45°C. These simplifications could produce systematic (seasonal dependence) and random errors (Schneider et al., 2008a; Redondas et al., 2014). In fact, as noted by Redondas et al. (2014) and recently confirmed by Gröbner et al. (2021), the operational ozone absorption coefficient of Brewer spectroradiometers is, albeit weakly, sensitive to a change in effective ozone temperature

of about 0.1% per 10K with respect to the ozone absorption cross-sections measured by the University of Bremen (IUP) in 2013 (Serdyuchenko et al., 2014). At IZO, differences between the assumed and actual effective temperatures as high as 10K or even greater are observed in the winter months. Note that the dataset IUP has been selected by the WMO as the future new reference cross-sections for the Brewer and Dobson networks (Gröbner et al., 2021).

It should be noted that, as documented in Arosa and Davos stations (Gröbner et al., 2021), the impact of the seasonal variability of effective O₃ height (between 20.2-23.8 km) on the calculation of the ozone slant path is at most 0.3% at an air mass of 3.9 (solar zenith angle, SZA, of 76°), which is the maximum that can be reached due to the mountains blocking the horizon at both sites.

Therefore, all these factors are contributing to the differences observed between FTIR and Brewer data at a seasonal scale and will be further explained in the revised manuscript, in accordance with the Referee's suggestion. The seasonal sensitivity of the FTIR retrievals will be briefly discussed in Section 3.2.1, while the Brewer seasonal sensitivity will be further detailed in Section 4.1.

Lines 419-421: it is claimed that the best performance is for set-ups using narrow windows and temperature fits for upper tropospheric region. To my point of view, the setup 1000T seems to be more appropriate for this region (Figure 9). The authors might want to distinguish the best set-up appropriated for different specific altitudes.

The FTIR and ECC comparison (Section 4.2) largely discusses the vertical performance of the different set-ups. In fact, the section concludes with the statement mentioned by the Referee, i.e., “the best performance is overall documented for the set-ups using narrow micro-windows and simultaneous temperature fit up to the upper troposphere region.” However, it also recognises that “beyond these altitudes, the broad micro-window strategy seems to provide the best agreement with respect to ECC data”. In this sense, the authors have sought to present and discuss the results obtained, but we do not find it appropriate to recommend different set-ups depending on altitude ranges as this recommendation could be confusing and not practical for operational retrievals within the NDACC FTIR community.

Regarding the best set-ups for the troposphere region, following Referee#2's suggestion, the vertical comparison based on integrated partial columns is expected to be more robust as wider layers are then less dependent on the FTIR vertical sensitivity than a single altitude on the profile. Therefore, the FTIR and ECC comparison at representative altitudes will be replaced with the comparison between ozone partial columns using the altitude levels as defined in García et al. (2012), i.e., the layers that are sufficiently well-detectable by the ground-based FTIR system (2.37-13 km, 12-23 km and 22-29 km). Accordingly, Table 3 of the preprint will be replaced by the following Table and the discussion of Section 4.2 will be modified.

As shown Table 2 below (and Figure 9 of the preprint), the bias with respect to the smoothed ECC partial columns is effectively smaller for the 1000/1000T set-ups. However, the broadband strategies overall provide much scatter than those using narrow micro-windows. See, for example, the comparison results for the 2008-2018 period, which can be considered as reference given the better instrumental alignment and the greater number of FTIR-ECC coincidences.

set-up	1999-2004	2005-2008	2008-2018	1999-2018
	M[%], σ [%], R			
FTIR-ECC at 2.37-13 km				
1000	15.86, 7.08, 0.934	11.44, 6.58, 0.956	9.08, 5.46, 0.970	10.63, 6.61, 0.953
4MWs	15.08, 7.11, 0.937	12.08, 6.54, 0.958	9.38, 5.10, 0.974	10.62, 6.46, 0.956
5MWs	16.24, 7.09, 0.938	12.30, 6.64, 0.957	9.72, 5.13, 0.974	10.89, 6.56, 0.956
1000T	15.05, 7.30, 0.934	10.39, 6.73, 0.954	8.12, 5.45, 0.971	10.00, 6.67, 0.953
4MWsT	15.56, 7.22, 0.938	11.56, 6.76, 0.957	9.26, 4.94, 0.975	10.54, 6.36, 0.958
5MWsT	16.93, 7.05, 0.940	12.76, 6.82, 0.956	10.11, 4.99, 0.976	11.20, 6.42, 0.958
FTIR-ECC at 12-23 km				
1000	17.30, 5.76, 0.914	16.01, 4.54, 0.946	13.23, 4.70, 0.959	14.59, 5.23, 0.944
4MWs	17.91, 5.58, 0.928	15.99, 4.86, 0.943	13.41, 4.82, 0.961	14.79, 5.29, 0.947
5MWs	17.89, 5.43, 0.939	16.03, 4.94, 0.943	13.72, 4.81, 0.962	14.91, 5.21, 0.951
1000T	16.83, 5.64, 0.921	15.19, 4.59, 0.945	12.13, 4.75, 0.961	13.72, 5.27, 0.946
4MWsT	17.25, 5.61, 0.930	16.44, 4.65, 0.947	14.18, 4.73, 0.963	15.30, 5.12, 0.951
5MWsT	17.48, 5.72, 0.935	16.91, 4.67, 0.948	15.07, 4.77, 0.963	16.02, 5.11, 0.953
FTIR-ECC at 22-29 km				
1000	15.92, 3.71, 0.820	16.23, 2.87, 0.888	13.94, 3.17, 0.756	14.76, 3.50, 0.779
4MWs	16.09, 4.01, 0.793	16.67, 2.88, 0.888	14.16, 3.21, 0.767	14.80, 3.64, 0.773
5MWs	16.00, 4.10, 0.783	16.43, 2.87, 0.892	14.06, 3.23, 0.777	14.79, 3.68, 0.776
1000T	16.80, 3.54, 0.866	15.56, 3.12, 0.856	13.88, 3.22, 0.735	14.51, 3.55, 0.778
4MWsT	16.28, 3.56, 0.864	15.61, 3.36, 0.844	14.45, 3.05, 0.774	14.96, 3.43, 0.801
5MWsT	16.31, 3.67, 0.856	15.28, 3.53, 0.829	14.47, 3.12, 0.775	15.06, 3.50, 0.798

Table 2: Summary of statistics for the FTIR-smoothed ECC comparison for the O₃ partial columns computed between 2.37-13 km, 12-23 km, and 22-29 km for the set-ups 1000/1000T, 4MWs/4MWsT, and 5MWs/5MWsT: median (M, in %) and standard deviation (σ , in %) of the relative differences, and Pearson correlation coefficient (R) of the direct comparison for the periods 1999-2004, 2005-May 2008 and June 2008-2018, and for the entire time series (1999-2018). The number of coincident FTIR-ECC measurements is 56, 49, and 167 for the three periods, respectively, and 272 for the whole dataset.

Section 3.2.2 is hard to follow and needs to be rewriting to easily analyze Figure 4.

Following Referee#3's suggestion, Section 3.2.2 will be revised and simplified to allow for an easy read. Figure 4 will be simplified and combined with Figure 5, and the discussion and plots showing the detailed error analysis based on the different error sources will be moved to Appendix A.

Line 224-225: According to Figure 4, the measurement noise and ILS are between 0.1 to 0.6%, not 0.1-0.2%

The statistical contributions of the measurement noise and ILS function are between 0.1-0.2% provided the simultaneous atmospheric temperature retrieval is not included in the O₃ retrieval

strategy, i.e., for the set-ups 1000, 4MWs and 5MWs. However, as the Referee mentioned, they indeed increase up to 0.6% when the temperature fit is taken into account due to the significant cross-interference introduced by temperature. This explanation is included between lines 224-228 in the original manuscript, but it has been explained in greater detail in the revised text as follows:

The FTIR measurements acquisition takes 10 minutes as stated in the manuscript. Why choosing a coincidence criterion of 5 minutes when comparing the Brewer to the FTIR data? What is the expected temporal variability of O₃ at IZO within 5 minutes?

Given that the differences among the FTIR set-ups are expected to be small, a strict coincidence criterion might be recommendable to minimise the influence of external factors on the comparisons (e.g. the natural variability of O₃). Following this idea, a temporal window equal to half the duration of the FTIR O₃ measurements has been selected for this work, this being 5 minutes. Therefore, only those Brewer observations taken within ± 5 minutes around the midpoint of each FTIR observation (chosen as reference time) have been paired. Although this temporal collocation is very restrictive, the number of coincidences is robust enough to obtain reliable results, and well-representative of the entire FTIR time series. Note that a 5 min window has been used in other studies when looking at very precise comparisons (e.g. between Brewer and Dobson measurements in Gröbner et al., 2021).

Figure 4 shows the temporal variability of O₃ total columns (TC) as observed by Brewer spectrometer at IZO within different temporal windows. As observed, only temporal intervals less than 10 minutes ensure that natural O₃ variations are limited to less than 0.15%, which is within the expected differences among the FTIR set-ups. These results are similar to those obtained at the Arosa station, where a repeatability of 0.15% within 10 minutes was found for Brewer O₃ observations (Scarnato et al., 2010).

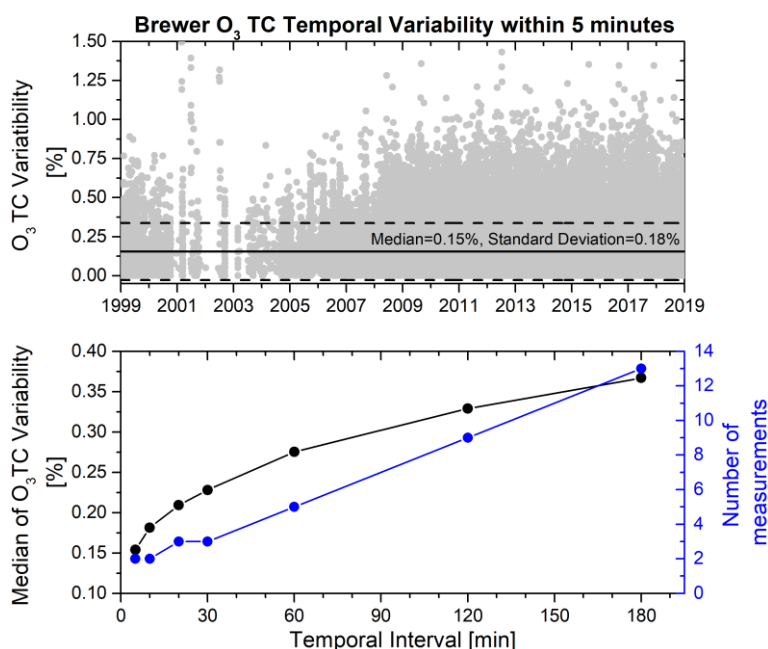


Figure 4. (a) Time series of the O₃ total column (TC) variability within 5 minutes as observed by Brewer spectrometer at IZO. Solid and dashed lines represent median values and $\pm 1\sigma$ ranges, respectively. (b) Median of O₃ TC variability, and number of measurements, within different temporal intervals (in minutes).

Technical comments:

Line 221: change “do depent” to “do depend”

Figure 4: rephrase legend to 1000T, MW4T similarly to the other figures.

Line 264: to ‘summarize’ instead of to ‘sum up’.

All technical comments have been corrected in the revised manuscript according to the Referee’s suggestions.

References

- García, O. E., Schneider, M., Redondas, A., González, Y., Hase, F., Blumenstock, T., and Sepúlveda, E.: Investigating the long-term evolution of subtropical ozone profiles applying ground-based FTIR spectrometry, *Atmospheric Measurement Techniques*, 5, 2917–2931, <https://doi.org/10.5194/amt-5-2917-2012>, 2012.
- García, O. E., Schneider, M., Hase, F., Blumenstock, T., Sepúlveda, E., and González, Y.: Quality assessment of ozone total column amounts as monitored by ground-based solar absorption spectrometry in the near infrared ($>3000\text{ cm}^{-1}$), *Atmospheric Measurement Techniques*, 7, 3071–3084, <https://doi.org/10.5194/amt-7-3071-2014>, 2014.
- Gaudel, A., Cooper, O., Ancellet, G., Barret, B., Boynard, A., Burrows, J., Clerbaux, C., Coheur, P.-F., Cuesta, J. and Cuevas, E., Doniki, S., Dufour, G., Ebojje, F., Foret, G., García, O., Granados Muños, M., Hannigan, J., Hase, F., Huang, G., Hassler, B., Hurtmans, D., Jaffe, D., Jones, N., Kalabokas, P., Kerridge, B., Kulawik, S., Latter, B., Leblanc, T., Le Flochmoën, E., Lin, W., Liu, J., Liu, X., Mahieu, E., McClure-Begley, A., Neu, J., Osman, M., Palm, M., Petetin, H., Petropavlovskikh, I., Querel, R., Rahpoe, N., Rozanov, A., Schultz, M., Schwab, J., Siddans, R., Smale, D., Steinbacher, M., Tanimoto, H., Tarasick, D., Thouret, V., Thompson, A., Trickl, T., Weatherhead, 1075 E., Wespes, C., Worden, H., Vigouroux, C., Xu, X., Zeng, G., and Ziemke, J.: Tropospheric Ozone Assessment Report: Present-day distribution and trends of tropospheric ozone relevant to climate and global atmospheric chemistry model evaluation, *Elementa: Science of the Anthropocene*, 6, 2018.
- Gröbner, J., Schill, H., Egli, L., and Stübi, R.: Consistency of total column ozone measurements between the Brewer and Dobson spectroradiometers of the LKO Arosa and PMOD/WRC Davos, *Atmospheric Measurement Techniques*, 14, 3319–3331, <https://doi.org/10.5194/amt-14-3319-2021>, 2021.
- Redondas, A., Evans, R., Stuebi, R., Köhler, U., and Weber, M.: Evaluation of the use of five laboratory-determined ozone absorption cross sections in Brewer and Dobson retrieval algorithms, *Atmospheric Chemistry and Physics*, 14, 1635–1648, <https://doi.org/10.5194/acp-14-1635-2014>, 2014.
- Scarnato, B., Staehelin, J., Stübi, R., and Schill, H.: Long-term total ozone observations at Arosa (Switzerland) with Dobson and Brewer instruments (1988–2007), *J. Geophys. Res.-Atmos.*, 115, D13306, doi:10.1029/2009JD011908, 2010.
- Schneider, M., Barthlott, S., Hase, F., González, Y., Yoshimura, K., García, O. E., Sepúlveda, E., Gomez-Pelaez, A., Gisi, M., Kohlhepp, R., Dohe, S., Blumenstock, T., Wiegeler, A., Christner, E., Strong, K., Weaver, D., Palm, M., Deutscher, N. M., Warneke, T., Notholt, J., Lejeune, B., Demoulin, P., Jones, N., Griffith, D. W. T., Smale, D., and Robinson, J.: Ground-based remote sensing of tropospheric water vapour isotopologues within the project MUSICA, *Atmospheric Measurement Techniques*, 5, 3007–3027, <https://doi.org/10.5194/amt-5-3007-2012>, 2012.
- Serdyuchenko, A., Gorshelev, V., Weber, M., Chehade, W., and Burrows, J. P.: High spectral resolution ozone absorption crosssections – Part 2: Temperature dependence, *Atmospheric Measurement Techniques*, 7, 625–636, <https://doi.org/10.5194/amt-7-625-2014>, 2014
- Steinbrecht, W., Froidevaux, L., Fuller, R., Wang, R., Anderson, J., Roth, C., Bourassa, A., Degenstein, D., Damadeo, R., Zawodny, J., Frith, S., McPeters, R., Bhartia, P., Wild, J., Long, C., Davis, S., Rosenlof, K., Sofieva, V., Walker, K., Rahpoe, N., Rozanov, A., Weber, M., Laeng, A., von Clarmann, T., Stiller, G., Kramarova, N., Godin-Beekmann, S., Leblanc, T., Querel, R., Swart, D., Boyd, I., Hocke, K., Kämpfer, N., Maillard Barras, E., Moreira, L., Nedoluha, G., Vigouroux, C., Blumenstock, T., Schneider, M., García, O., Jones, N., Mahieu, E., Smale, D., Kotkamp, M.,

Robinson, J., Petropavlovskikh, I., Harris, N., Hassler, B., Hubert, D., and Tummon, F.: An update on ozone profile trends for the period 2000 to 2016, *Atmospheric Chemistry and Physics*, 17, 10 675–10 690, <https://doi.org/10.5194/acp17-10675-2017>, 2017

Vigouroux, C., Blumenstock, T., Coffey, M., Errera, Q., García, O., Jones, N. B., Hannigan, J. W., Hase, F., Liley, B., Mahieu, E., Mellqvist, J., Notholt, J., Palm, M., Persson, G., Schneider, M., Servais, C., Smale, D., Thölix, L., and De Mazière, M.: Trends of ozone total columns and vertical distribution from FTIR observations at eight NDACC stations around the globe, *Atmospheric Chemistry and Physics*, 15, 2915–2933, <https://doi.org/10.5194/acp-15-2915-2015>, 2015.

WMO: Scientific Assessment of Ozone Depletion: 2018, Global Ozone Research and Monitoring Project–Report No. 58, Tech. rep., World Meteorological Organization, Geneva, Switzerland, 2018.